# Parent Material, Elemental Composition, and Pedogenic Processes in Ophiolitic Soils in Eastern Taiwan

**Marvin Decenilla Cascante, Cho Yin Wu, Chia Yu Yang, Hui Zhen Hum and Zeng Yei Hseu***

*Department of Agricultural Chemistry, National Taiwan University, Taipei 10617, Taiwan*

## ABSTRACT

The ophiolite complex in Chishang, Eastern Taiwan, exhibits a wide variety of soil parent materials, resulting in notable variations in elemental composition and pedological properties. This study characterized soils from four pedons along a toposequence, focusing on mineral composition, micromorphology, general properties, and elemental composition. A mass balance model quantified the mobility of clay, along with major and trace elements. The soils predominantly comprised chlorites, feldspars, quartz, micas, and calcite, with higher silica (Si) concentrations followed by Al. Some of the studied soils had elevated Ca/Mg ratios ($\geq 1.0$), indicating a primary derivation from sedimentary parent material, such as mudstone. However, concentrations of Cr (71.2 to 105.0 mg kg$^{-1}$), Ni (43.2 mg kg$^{-1}$), and Co (20.3 to 27.9 mg kg$^{-1}$) were notably lower than those reported in other global studies on ophiolite complexes. A significant and positive correlation occurred between Fe- and Al-oxides and Cr, Ni, and Co. The poor correlations between these trace metals and other soil properties (pH, organic carbon, Ca/Mg ratio, rare earth elements) suggest that these factors had limited influence on Cr, Ni, and Co concentrations. The strong ($p < 0.01$) correlations among trace metals indicate a genetic linkage formed during soil development rather than anthropogenic activities. Additionally, trace metal enrichment in surface soils, as evidenced by the increase of clay and Fe/Al oxides, implies that these components provide crucial adsorption sites for Cr, Ni, and Co.

*Keywords*: Mass balance, mudstone, ophiolitic soils, pedogenesis, trace metals

## INTRODUCTION

Ophiolites originate from the oceanic crust and upper mantle and are primarily emplaced along continental margins through complex tectonic processes. These geological formations are characterized by their association with significant tectonic movements, often observed in regions with

active plate boundaries. Soils derived from ophiolites are relatively rare on the Earth's surface, mainly found near tectonic plate boundaries such as those in the circum-Pacific region and the Mediterranean (DiPietro, 2013; Dilek & Furnes, 2014). Despite their limited distribution, soils in ophiolite complexes are of great scientific interest because they offer valuable insights into the sources of detrital materials, geodynamic processes, and soil formation scenarios (Bédard et al., 2019; Gawlick & Missoni, 2019; Robertson et al., 2020). For instance, the elemental composition of soils within the ophiolite complex in eastern Taiwan, which originated from marine sediments during the convergence of the Eurasian continental and Philippine oceanic plates, was significantly influenced by pedogenic processes, topographic position, and the composition of the parent material (Cheng et al., 2009). The concept of parent material, referring to the original rock types from which the components of an ophiolite are derived, is central to understanding these soils' chemical and mineralogical properties.

Soils from ophiolite complexes typically exhibit considerable variation in the geochemical concentrations of trace metals. For example, in the soils of the Zhob Valley in Pakistan, the total concentrations of chromium (Cr; 588–1929 mg kg$^{-1}$), nickel (Ni; 665–1725 mg kg$^{-1}$), and cobalt (Co; 2.5–14.5 mg kg$^{-1}$) were several times higher than those found in benchmark soils, where Cr, Ni, and Co concentrations were 34.8 mg kg$^{-1}$, 541 mg kg$^{-1}$, and 1.2 mg kg$^{-1}$, respectively (Ullah & Muhammad, 2020). In addition, serpentinites, which form a significant part of ophiolites, are primarily composed of serpentine minerals such as antigorite, lizardite, and chrysotile, along with other minerals like talc, calcite, brucite, chlorite, magnetite, and chromite (Hseu et al., 2018; Yang et al., 2022). Besides their high concentrations of Cr, Ni, and Co, soils from ophiolitic complexes often exhibit low calcium (Ca) to magnesium (Mg) ratios and reduced levels of essential macronutrients, including nitrogen (N), phosphorus (P), and potassium (K). These characteristics contribute to the development of unique flora and distinct soil properties, which can significantly affect local ecosystems (Hseu et al., 2018; Merrot et al., 2021; Tazikeh et al., 2018; Yang et al., 2022). The low Ca/Mg ratio, coupled with the high trace metal concentrations, presents significant challenges to agricultural productivity in these regions (Hseu et al., 2018).

The origin and landscape of soils within ophiolite complexes are closely linked to their marine sedimentary origins, leading to distinct variations in elemental composition and pedological characteristics. Hseu et al. (2007) reported that the concentrations of Cr and Ni in soils derived from serpentinites were five to ten times higher than those in soils derived from mixed mudstones in an ophiolite complex in Eastern Taiwan. The finding underscores the critical role of parent material in determining the geochemical composition of soils derived from sedimentary sources and the behavior of these elements under various environmental conditions (Tazikeh et al., 2018). In addition to the parent material, various soil properties, including pH, the presence of iron (Fe) oxides (Fe$_2$O$_3$), Fe sulfides, Fe-

bearing clay minerals, manganese (Mn), and organic matter (OM) play significant roles in controlling the distribution of trace metals in terrestrial environments (Bolaños-Benitez et al., 2021; Merrot et al., 2021; Rinklebe & Shaneen, 2017). At low pH, Cr is reduced and adsorbed onto the surfaces of OM and Fe oxides, forming highly stable and less mobile Cr (III) species (Baralkiewicz & Siepak, 1999).

However, Mn acts as a critical oxidant, forming the toxic and carcinogenic Cr (VI) species at high pH (Hseu, 2018; Merrot et al., 2021; Morrison et al., 2015). Similarly, the solubility and mobility of Ni and Co increase with decreasing soil pH, with Ni (II) and Co (II) being the more stable species under varying pH levels and oxidation-reduction conditions (Ma & Hooda, 2010). The mass balance model has determined the geochemical behaviors of trace metals in soils (da Silva et al., 2020; Ito et al., 2021; Wu et al., 2024). This model accounts for the addition, removal, and redistribution of elements within a soil profile relative to its parent material, making it a critical tool for understanding the fate of trace metals during soil formation and evolution (Chadwick et al., 1990; Hum et al., 2024; Wu et al., 2023). In addition to trace metals, mass balance models have been widely applied to major elements, providing insights into the interactions of these components within the soil system (da Silva et al., 2020; Ito et al., 2021; Hum et al., 2024; Wu et al., 2023; Wu et al., 2024).

Despite the importance of the mass balance approach, limited studies have specifically applied it to investigate the mobility and distribution of Cr, Ni, Co, and other major elements during soil formation, particularly in soils derived from sedimentary parent materials, such as those found in ophiolitic complexes. Applying mass balance models provides a valuable approach for evaluating the behavior of trace metals and major elements in ophiolitic soils, allowing quantification of the rate of gains and losses of elements throughout the soil profile, thereby revealing the processes that influence their distribution and mobility. These rates were measured relative to the immobile element, such as titanium (Ti), which remains stable and provides a reference point during weathering (Chapman & Horn, 1968; Egli et al., 2008; Harnois, 1988; Hum et al., 2024; Wu et al., 2023). This approach offers critical insights into mechanisms such as leaching, which removes soluble metal forms; adsorption onto clay minerals; complexation with various inorganic ligands; and secondary mineral formation that can immobilize metals under certain conditions (Chadwick et al., 1990; da Silva et al., 2020; Hum et al., 2024; Ito et al., 2021; Wu et al., 2023).

Studies on soils from ophiolite complexes have advanced significantly, with a focus on the environmental impact of trace metals and their elemental composition. These studies have highlighted the dual role of these soils: They can be relevant for agriculture yet pose undeniable threats to environmental sustainability due to their unique chemical properties (Hseu, 2018; Morrison et al., 2015; Yang et al., 2022). Understanding the geochemical background concentrations and distribution of major and trace elements in ophiolitic soils

Pertanika J. Trop. Agric. Sci. 48 (3): 991 - 1017 (2025)

993

is essential for effective pedological and environmental assessments, providing valuable information for land management and conservation efforts (Hseu et al., 2018). This study was conducted (1) to identify and characterize the parent materials of ophiolitic soils from Eastern Taiwan, (2) to analyze the elemental composition of these soils, (3) to explore the relationships between trace metals and pedogenic factors, and (4) to assess the mobility of soil components in these complex and dynamic environments.

## MATERIALS AND METHODS

### Site Description and Sampling

The study area was located in the ophiolite complex that belongs to the Miocene-aged Lichi Formation in the township of Chishang, Taiwan (Figure 1) (Ho, 1988). Four soil pedons along the south-facing gradient transect were selected from the summit (CP1), upper backslope (CP2), lower backslope (CP3), and foot slope (CP4) with elevation ranges from 290 to 343 m above sea level (Table 1). The climate condition of the study site is tropical humid, with massive rainfall and tropical cyclones from May to September. The mean annual air temperature is 22.5 °C, and the average rainfall is 1800 mm. The soil moisture and
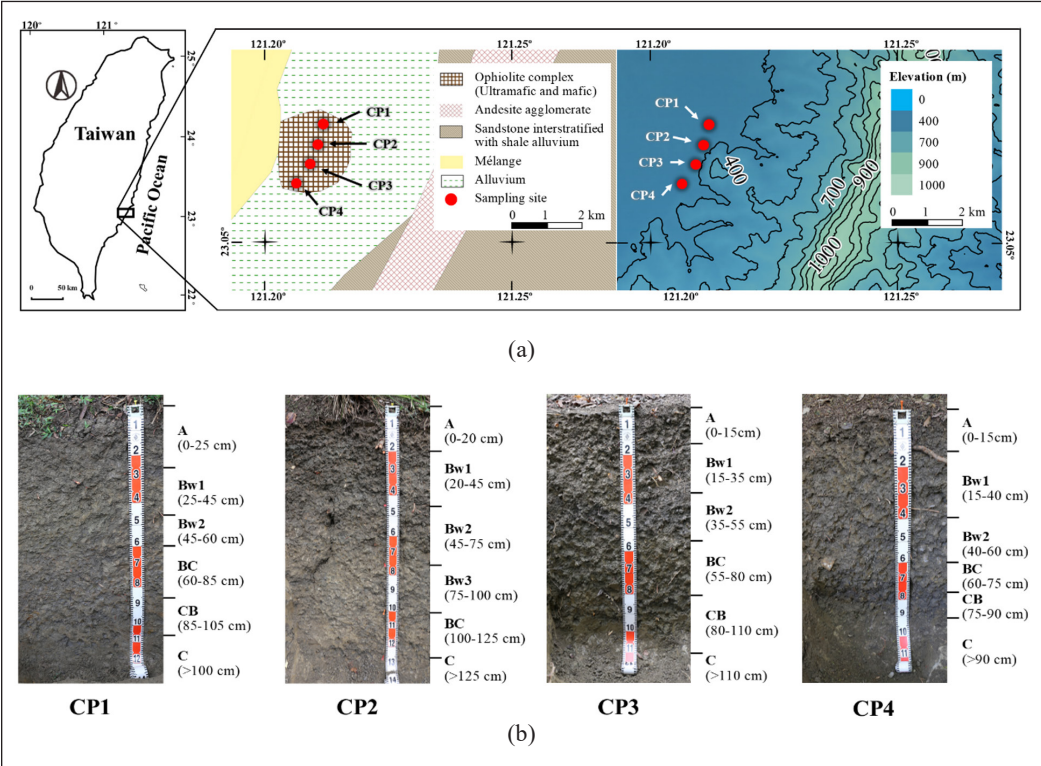


*Figure 1.* (a) Location of the studied soils and their geological and topographic map; and (b) studied pedons (CP1-summit, CP2-upper backslope, CP3-lower backslope, and CP4-footslope)

Table 1

*Geographic information and classification of the studied pedons*

| Pedon | Location | Elevation m | Slope % | Landscape Position | Soil Classification[1] |
|---|---|---|---|---|---|
| CP1 | N 23° 04' 16.82", E 121° 13' 21.64" | 343 | 15 | Summit | Typic Dystrudept |
| CP2 | N 23° 04' 11.95", E 121° 13' 16.34" | 322 | 15 | Upper backslope | Typic Dystrudept |
| CP3 | N 23° 04' 10.05", E 121° 13' 14.72" | 310 | 10 | Lower backslope | Typic Dystrudept |
| CP4 | N 23° 04' 09.21", E 121° 13' 11.04" | 290 | 5 | Foot slope | Typic Dystrudept |

*Note.* [1] Soil Taxonomy (Soil Survey Staff, 2022)

temperature regimes are udic and hyperthermic, respectively. The vegetation is dominated by tropical deciduous trees (*Annonaceae* sp.), exotic trees (*Leucaena leucocephala*), and perennial grasses (*Oplismenus hirtellus*, *Carex obnupta*, *Cortaderia jubata*, and *Saccharum spontaneum*). The field morphological description was determined according to the protocol suggested by the U.S. Soil Survey Manual (Soil Science Division Staff, 2017). The soil samples were collected according to genetic horizons, air-dried, and gently crushed to pass a 2-mm sieve for laboratory analyses.

## Characterization of the Studied Soil

The bulk density (Bd) was measured using the core method (Blake & Hartge, 1986). The pH was measured using a mixture of soil and deionized water (1:1, w/v) with a glass electrode (McLean, 1982). The Walkley-Black wet oxidation method was used to determine the organic carbon (OC) content (Nelson & Sommers, 1982). Cation exchange capacity (CEC) and base saturation (BS) percentage were determined by the ammonium acetate method (pH 7.0) (Rhoades, 1982). The particle-size distribution of the soil samples was determined using the pipette method (Gee & Bauder, 1986). Dithionite-citrate-bicarbonate (DCB) extraction was used to determine the dissolved crystalline and noncrystalline Fe- and Al-oxides (Mehra & Jackson, 2013).

The total concentrations of silicon dioxide ($SiO_2$), aluminum oxide ($Al_2O_3$), $Fe_2O_3$, potassium oxide ($K_2O$), calcium oxide (CaO), magnesium oxide (MgO), sodium oxide ($Na_2O$), manganese oxide (MnO), and titanium dioxide ($TiO_2$) were determined after the following pretreatment of the sample procedure: A soil sample of 0.6 g (<75 μm) was combined with 6.0 g of flux composed of 49.75% $Li_2B_4O_7$, 49.75% $LiBO_2$, and 0.50% LiBr in a Pt-Au crucible. The mixture was fused using a fusion instrument (Claisse M4, Malvern Panalytical, UK) for 13 min with a liquefied petroleum gas and air flame. After fusion, the clear melt was poured into a 32 mm Pt-Au mold and cooled to room temperature. The uniform fused glass disk was used to determine major elements using a wavelength-dispersive X-ray fluorescence spectrometer (WDXRF; Axios^mAX Advanced WDXRF, Malvern Panalytical, UK).

The total concentrations of trace elements (Cr, Ni, and Co) were measured following digestion with a mixture of HF- $HNO_3$-HCl, as outlined in the U.S. Environmental Protection Agency's protocol (method 3052; U.S. Environmental Protection Agency, 2021). The digestion process was associated with a microwave oven system (Speedwave Entry, Berghof, Germany) at a gradual temperature increase of 180 °C in 10 min and further sustained at the same temperature and time. The concentration of all major and trace elements in the extraction and digestion solutions was quantified using inductively coupled plasma optical emission spectroscopy (ICP-OES; Optima 2100DV, PerkinElmer, Waltham, USA).

**Mineralogical and Micromorphological Analyses**

The powdered sand fractions (0.05–2 mm) by the pipette method were used for the mineral composition determination of the parent materials using X-ray diffraction (XRD, MiniFlex 600 Powder Diffractometer, Rigaku, Japan). The XRD patterns of the samples were obtained from 0º to 70º 2θ at a scanning rate of 10º 2θ min$^{-1}$. Furthermore, micromorphological characteristics and primary minerals were identified on thin sections of soil with a polarized light microscope (DM2700 M, Leica, Germany).

**Elemental Mass Balance Calculation**

The elemental mass balance approach was applied to estimate the gain and loss of the clay fractions, major elements (Si, Al, Fe, Ca, and Mg), and trace metals (Cr, Ni, and Co) in the studied pedons. The mass variation of the target element (j) was compared with the relative immobile index element (i) with the consideration of soil volume changes during soil development. Strain [$\varepsilon$], which stands for the volume change, was calculated based on the following equation (Brimhall & Dietrich, 1987; Brimhall et al., 1992; Chadwick et al., 1990):

$$\varepsilon_{i,w} = (\rho_p C_{i,p} / \rho_w C_{i,w}) - 1 \qquad [1]$$

where subscripts $p$ and $w$ represent the parent material and the weathered soil, respectively. $\rho$ stands for Bd, while $C$ refers to target and index element concentration. $\varepsilon$ was employed to get the mobility of the target element (j) in the soils. The mass transfer coefficient ($\tau_{j,w}$) was calculated, followed by the equation below:

$$\tau_{j,w} = ((\rho_w C_{j,w} / \rho_p C_{j,p})( \varepsilon_{i,w}+1)) - 1 \qquad [2]$$

where the positive value indicates the net gain of the target element (j) related to the parent material while the negative value represents the net loss, in Equations 1 and 2, C horizons in the studied pedons were regarded as the parent material, and Ti was employed as the immobile index element in the calculations.

**Quality Assurance and Control and Statistical Analysis**

A standard reference material, SRM 2709a (San Joaquin Soil) from the National Institute of Standards and Technology (NIST), USA, was also digested and analyzed using the U.S. Environmental Protection Agency (2021). The recoveries of the trace metals were as follows: Cr, 104%; Ni, 89.6%; Co, 94.60%. Additionally, a certified reference material, BCR-2 (Columbia River Basalt) from the United States Geological Survey, was also analyzed using WDXRF. The recoveries of targeted elements from the BCR-2 were as follows: Si, 99.6%; Ti, 100%; Al, 100%; Fe, 99.9%; Mn, 101%; Mg, 99.6%; Ca, 100%; Na, 110%; and K, 101%. For every 10 sample sets, a blank and spiked procedure was performed for interference assessment and contamination check.

Statistical software R (version 4.1.0) was used to perform Pearson's correlation coefficient ($r$) analysis for the linear correlation among soil properties. The statistical significance levels are as follows: $*p < 0.05$, $**p < 0.01$, and $***p < 0.001$.

## RESULTS AND DISCUSSION

### Parent Material and Micromorphology

This study utilized XRD to identify the primary minerals present in the sand fractions of ophiolitic soil. That is, chlorites were identified by peaks at 1.44, 0.72, 0.48, 0.46, and 0.15 nm; feldspars were characterized by peaks at 0.64, 0.43, 0.39, and 0.38 nm; quartz was indicated by peaks at 0.25, 0.18, and 0.17 nm; micas were identified from peaks at 1.00, 0.33, and 0.20 nm; and calcite was observed from peaks at 0.23 and 0.17 nm (Figure 2). The abovementioned minerals suggested a complex mineralogical composition that deviates from the typical ophiolite parent materials. Ophiolites were generally expected to be composed mainly of minerals such as serpentinized amphibole, pyroxene, and accessory olivine, which reflect the soils developed, particularly those that have not undergone extensive weathering (Dilek & Furnes, 2014; Külah et al., 2014). However, the dominance of chlorites, feldspars, quartz, micas, and calcite in the studied soils indicated that they were predominantly derived from other parent materials rather than serpentinites. Instead, the mineralogy of these soils suggested a significant influence from marine sediments, particularly mudstones, which were known to contribute to the mineral diversity found in ophiolitic soil profiles (Hseu et al., 2007; Külah et al., 2014). Additionally, no slickensides or visible cracks, typically characteristic of soils derived from fine-textured marine sediments, were observed in the field, and this corresponded with the absence of smectite in the XRD results. Furthermore, the relatively lower number of peaks and peak intensities for serpentine (0.72 and 0.22 nm), chrysotile (0.36 and 0.15 nm), and talc (1.0, 0.31 and 0.25 nm) suggested that these minerals were present in smaller quantities than expected. However, kaolinite appears to be identified by the peaks at 0.72 nm and 0.36 nm in the XRD spectra, which are characteristic of soils derived from fine-grained marine sediments.
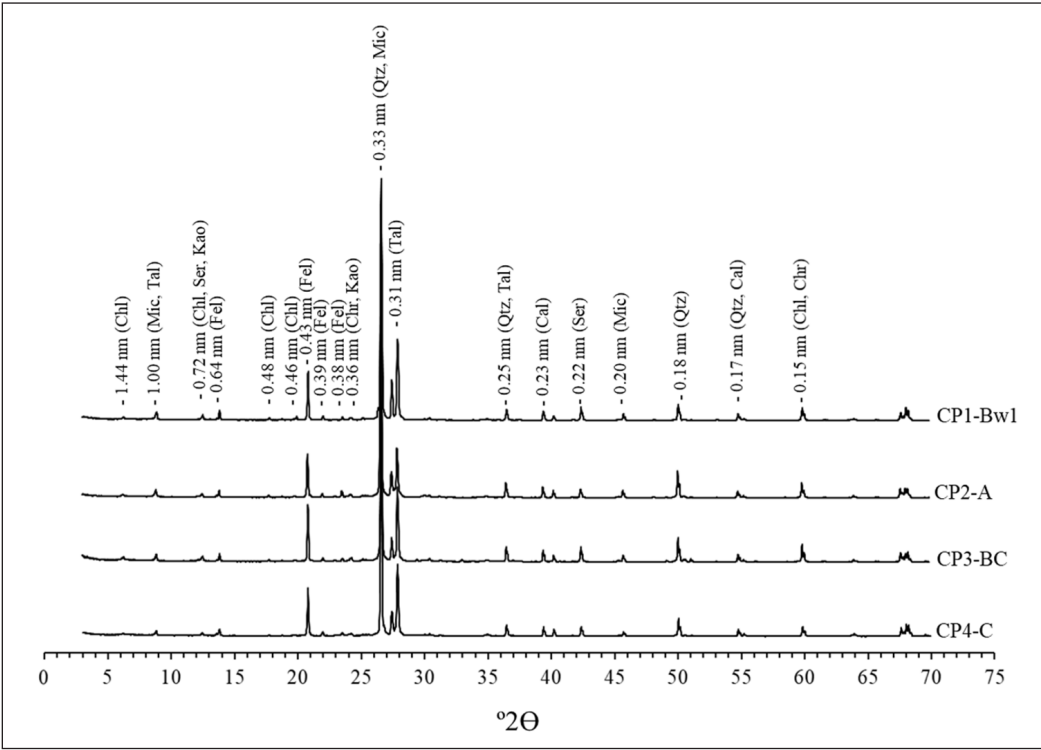
*Figure 2.* X-ray diffraction pattern of the sand fractions in ophiolite soils (CP1-Bw1, CP2-A, CP3-BC, and CP4-C). Chl = chlorite, Fel = feldspar, Qtz = quartz, Mic = micas, Ser = serpentine, Chr = chrysotile, Tal = talc, Kao = kaolinite

This observation is consistent with the findings of Hseu et al. (2007). Moreover, talc could also potentially overlap with mica near 1.00 nm. This indicated that the soils had been less influenced by serpentinites than one might anticipate, implying a more complex geological history involving altering the original ophiolitic materials during their formation. This alteration reflects the broader geological processes and environmental conditions that have impacted the ophiolite complex over time.

Plane-polarized light (PPL) and cross-polarized light (XPL) microscopy images verified the presence of minerals previously identified by XRD. Under PPL, chlorite was recognized by its colorless to pale green appearance, showcasing its pleochroic behavior as it changed intensity with the rotation of the microscope stage. When viewed under XPL, chlorite displayed striking blue interference colors, which is characteristic of this mineral (Figure 3a). Feldspar, which is a significant rock-forming mineral commonly found in ultramafic and sedimentary parent materials (Verrecchia & Trombino, 2021), was identified by its distinctive features. Under PPL, feldspar exhibited a tabular parallel habit with a cloudy color; under XPL, it showed a distinctive polysynthetic twinning pattern with interference colors ranging from gray to white (Figure 3a). Quartz was identified by
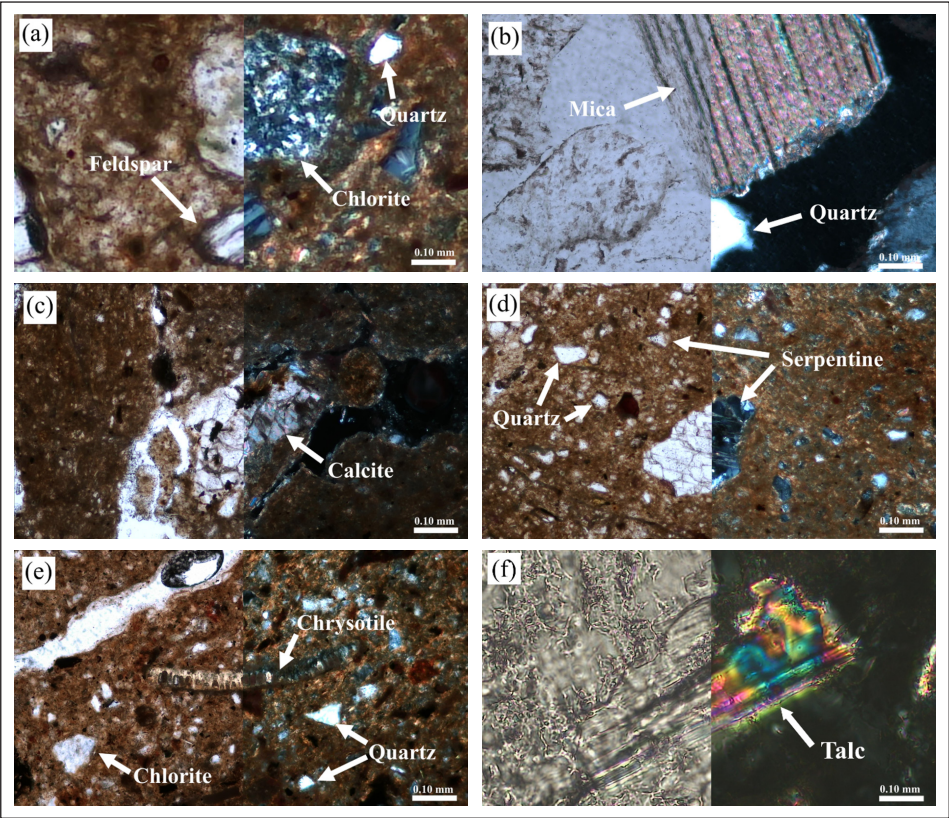
*Figure 3.* Photomicrographs of the thin section (left, plane polarized; right, cross-polarized light) showing: (a) chlorite, feldspar and quartz in Bw2 horizon of CP2 pedon; (b) quartz and micas from CB horizon of CP3 pedon; (c) calcite in Bw2 horizon of CP2 pedon; (d) quartz and serpentine in CB horizon of CP4 pedon; € chlorite, chrysotile, and quartz in A horizon of CP1 pedon; (f) and talc in Bw1 horizon of CP3 pedon

detrital grains that appeared colorless or white under both PPL and XPL. These grains were observed consistently across multiple photos (Figures 3a, 3b, 3d, and 3e), reinforcing the identification of quartz by the XRD. The presence of micas group minerals was indicated by laminar grains that showed brown to brownish-green colors with white to gray bands under PPL. Under XPL, these grains exhibited bright colors ranging from pink to green to blue (Figure 3b). This range of interference colors is typical for mica minerals and helps identify them. Calcite was identified by an aggregate of white grains with pink to gray borders under PPL. When observed under XPL, calcite displayed high-order interference colors, which are indicative of its high birefringence (Figure 3c). The identification of the primary minerals in the thin sections using polarized light microscopy was based on the mineralogical criteria described by Deer et al. (2013).

The thin sections also revealed the presence of serpentine, chrysotile, and talc. Serpentine minerals were identified by their platy texture, which appeared white under PPL

Pertanika J. Trop. Agric. Sci. 48 (3): 991 - 1017 (2025)

999

and showed gray to yellow interference colors under XPL. Chrysotile, a fibrous variety of serpentine, appeared with a parallel fibrous texture that was white in PPL and displayed gray to yellow colors under XPL (Figures 3d and 3e). Furthermore, the presence of talc was indicated by a flaky aggregate with an irregular bladed texture that appeared colorless with hints of very pale green under PPL. Under XPL, this aggregate displayed high third-order interference colors.

The detailed observations under PPL and XPL offer a comprehensive and conclusive verification of the mineral composition in the ophiolitic soils, providing nuanced insights that strongly corroborate the findings from XRD. The presence of tectosilicates such as feldspar and quartz, as well as phyllosilicate minerals like chlorite, serpentine group minerals, and micas, matches the expected outcomes. This evidence suggested that the parent materials of these soils were lithified, fine-grained sediment particles that weathered from various minerals and rocks, which underwent chemical alteration during tectonic movements (Macquaker et al., 1997; Lazar et al., 2015). Serpentine group minerals are generally not found in soils derived from sedimentary parent materials, particularly mudstone, due to their specific formation conditions (Perri et al., 2021). Their presence in the studied ophiolitic soils indicated a significant tectonic event and reflected the incorporation of primary minerals from serpentinites.

## Soil Physical and Chemical Characteristics

Table 2 provides a detailed overview of the selected soil characteristics across the studied ophiolitic soil pedons. The particle size distribution in these pedons showed no distinct variation, with the clay fraction consistently dominating. Specifically, the clay content ranged from 45.0% to 62.5%, surpassing the sand fraction, which varied between 2.5% and 40.0%. This trend was evident across all pedons, with the highest clay content observed in the lower backslope pedon (CP3) and the lowest in the foot slope pedon (CP4). The study further revealed that soil Bd tended to be lower in the surface horizons across all pedons compared to the subsurface horizons, indicative of the higher OM content (Jiménez-Ballesta et al., 2024). The soil pH values across the pedons were found to be slightly to moderately acidic, ranging from 6.1 to 6.9. Notably, these pH values remained consistent with increasing depth, suggesting a relatively uniform distribution of acidity throughout the soil profiles.

In terms of organic carbon (OC) content, the surface horizons exhibited relatively higher levels, ranging from 5.0% to 5.8%. The higher OC content in the surface horizons was attributed to the accumulation of OM, which is often deposited from plant litter and other organic inputs at the soil surface (Jiménez-Ballesta et al., 2024). Conversely, the OC content decreased with soil depth, ranging from 3.6% to 2.0% in the subsurface horizons. A notable observation was the consistently higher levels of exchangeable Ca compared

to Mg, K, and Na across all pedons. Exchangeable Ca ranged from 3.62 to 10.6 cmol(+) kg$^{-1}$, while Mg levels were lower, ranging from 0.45 to 1.12 cmol(+) kg$^{-1}$. The finding was somewhat unexpected, as soils developed in ophiolitic complex typically exhibit higher Mg levels than Ca (Hseu, 2018; Yang et al., 2022). The higher Ca levels in the studied soils suggested that they were primarily derived from sedimentary materials, namely calcite, which have a different elemental composition than ultramafic rocks. The CEC values in the studied pedons ranged from 14.5 to 27.3 cmol(+) kg$^{-1}$. The highest CEC value was recorded in the summit pedon (CP1), while the lowest was observed in the upper backslope pedon (CP2). The BS percentage in the studied soils ranged from 17.1% to 82.2%. Higher BS values were observed in the C horizons of all pedons, which was attributed to the leaching and accumulation of basic cations from the surface and subsurface soils into these deeper layers, highlighting the dynamic nature of nutrient cycling and soil development within the ophiolitic landscape.

The study also determined the contents of DCB extractable $Fe_d$ and $Al_d$, which ranged from 65.5 to 96.3 g kg$^{-1}$ and 5.04 to 11.8 g kg$^{-1}$, respectively (Table 2). Elevated concentrations of $Fe_d$ and $Al_d$ were particularly noticeable in the B horizons, where the accumulation of free Fe and Al oxides was more pronounced. The accumulation was likely due to the processes of weathering and leaching that preferentially concentrated these oxides in the subsurface horizons. Based on the observed soil characteristics, including the well-structured development in the mineral subsurface horizons (Bw) and the presence of low basic cations, the four studied pedons were classified as Typic Dystrudepts according to the Soil Survey Staff (2022)(Table 1).

**Total Content of Major and Trace Elements**

The total contents of major and trace elements in the studied pedons (CP1 to CP4) within the ophiolite complex are detailed in Table 3. Results showed that $SiO_2$ across the four pedons showed irregular fluctuations throughout the soil horizons, ranging from 65.8% to 53.2 %. Similarly, the concentrations of $Al_2O_3$ and $Fe_2O_3$ also exhibited vertical variations, with Al ranging from 16.8% to 13.5% and Fe from 6.59% to 4.52%. Notably, slightly higher levels of $Al_2O_3$ and $Fe_2O_3$ were observed in the CP2 pedon (located on the upper backslope) and the CP3 pedon (situated on the lower backslope). This was consistent with their topographic positions, which were typically zones of deposition where these elements could be accumulated. Moreover, results showed noticeably elevated concentrations of $Al_2O_3$ (15.1% to 16.8%) and $Fe_2O_3$ (5.41% to 6.45%) in B horizons, indicating the accumulation of the element during soil formation. In contrast, other selected elements, such as $K_2O$ (2.36% to 2.89%), $Na_2O$ (0.96% to 1.78%), MgO (1.51% to 2.31%), CaO (0.56% to 2.60%), and MnO (0.05% to 0.10%), were present in lower concentrations compared to $SiO_2$, $Al_2O_3$, and $Fe_2O_3$ across all pedons (Table 3). The elemental composition of the studied ophiolitic

Table 2
*Selected properties of the studied pedons*

| Pedon | Depth cm | Horizon | Sand | Clay % | $Bd^1$ g cm⁻³ | pH | $OC^2$ % | K | Na | Ca | Mg | $CEC^3$ | $BS^4$ % | $Fe_d^5$ | $Al_d^5$ g kg⁻¹ |
|---|---|---|---|---|---|---|---|---|---|---|---|---|---|---|---|
| | | | | | | | | | | Exchangeable bases cmol (+) kg⁻¹ | | | | | |
| CP1 | 0-25 | A | 17 | 50 | 1.4 | 6.3 | 4.97 | 0.20 | 0.02 | 3.91 | 0.60 | 27.3 | 17 | 78.4 | 10.7 |
| | 25-45 | Bw1 | 12 | 55 | 1.4 | 6.5 | 2.87 | 0.11 | 0.01 | 3.70 | 0.74 | 23.5 | 19 | 87.8 | 10.9 |
| | 45-60 | Bw2 | 10 | 55 | 1.5 | 6.8 | 2.54 | 0.11 | 0.01 | 4.10 | 0.82 | 20.6 | 24 | 78.4 | 9.97 |
| | 60-85 | BC | 12 | 52 | 1.6 | 6.6 | 2.08 | 0.11 | 0.04 | 3.93 | 0.85 | 19.7 | 25 | 76.1 | 8.75 |
| | 85-105 | CB | 30 | 45 | 1.6 | 6.8 | 1.86 | 0.12 | 0.09 | 6.62 | 0.90 | 16.4 | 47 | 75.9 | 7.30 |
| | >105 | C | 18 | 50 | 1.7 | 6.8 | 2.57 | 0.15 | 0.25 | 5.66 | 1.12 | 17.6 | 41 | 65.5 | 6.30 |
| CP2 | 0-20 | A | 10 | 55 | 1.5 | 6.6 | 4.99 | 0.22 | 0.05 | 6.69 | 0.60 | 24.4 | 31 | 75.1 | 7.78 |
| | 20-45 | Bw1 | 2.0 | 63 | 1.4 | 6.8 | 3.42 | 0.15 | 0.01 | 5.74 | 0.61 | 18.0 | 36 | 86.2 | 6.76 |
| | 45-75 | Bw2 | 15 | 58 | 1.5 | 6.6 | 3.08 | 0.13 | 0.02 | 6.64 | 0.77 | 17.8 | 43 | 84.2 | 6.18 |
| | 75-100 | Bw3 | 2 | 60 | 1.7 | 6.6 | 3.13 | 0.12 | 0.03 | 8.83 | 0.87 | 17.7 | 56 | 85.8 | 6.84 |
| | 100-125 | BC | 25 | 47 | 1.6 | 6.1 | 2.77 | 0.14 | 0.05 | 9.79 | 1.04 | 14.9 | 74 | 80.7 | 5.70 |
| | >125 | C | 15 | 45 | 1.7 | 6.6 | 3.16 | 0.14 | 0.06 | 10.6 | 1.11 | 14.5 | 82 | 85.5 | 5.04 |
| CP3 | 0-15 | A | 12 | 53 | 1.3 | 6.6 | 4.79 | 0.13 | 0.01 | 3.74 | 0.53 | 23.5 | 19 | 93.4 | 9.80 |
| | 15-35 | Bw1 | 17 | 58 | 1.4 | 6.9 | 2.80 | 0.10 | 0.01 | 3.95 | 0.57 | 22.4 | 21 | 93.2 | 10.8 |
| | 35-55 | Bw2 | 18 | 58 | 1.4 | 6.9 | 3.10 | 0.08 | 0.01 | 3.62 | 0.53 | 24.8 | 17 | 94.7 | 11.3 |
| | 55-80 | BC | 15 | 60 | 1.5 | 6.7 | 3.19 | 0.09 | 0.01 | 4.72 | 0.73 | 22.9 | 24 | 96.3 | 11.8 |
| | 80-110 | CB | 28 | 58 | 1.4 | 6.7 | 2.77 | 0.10 | 0.05 | 5.28 | 0.68 | 20.5 | 30 | 91.9 | 10.1 |
| | >110 | C | 13 | 60 | 1.5 | 6.7 | 2.74 | 0.10 | 0.02 | 6.93 | 0.71 | 19.4 | 40 | 91.6 | 10.9 |
| CP4 | 0-15 | A | 38 | 45 | 1.2 | 6.3 | 5.43 | 0.13 | 0.01 | 4.41 | 0.45 | 24.2 | 21 | 77.1 | 8.60 |
| | 15-40 | Bw1 | 30 | 50 | 1.6 | 6.5 | 2.95 | 0.17 | 0.02 | 5.29 | 0.54 | 20.3 | 30 | 85.6 | 9.81 |
| | 40-60 | Bw2 | 40 | 45 | 1.4 | 6.3 | 2.89 | 0.08 | 0.02 | 4.23 | 0.61 | 20.3 | 24 | 85.9 | 9.40 |
| | 60-75 | BC | 25 | 55 | 1.5 | 6.6 | 2.92 | 0.07 | 0.02 | 4.47 | 0.69 | 20.4 | 26 | 87.4 | 9.54 |
| | 75-90 | CB | 33 | 50 | 1.3 | 6.8 | 1.31 | 0.07 | 0.02 | 4.31 | 0.62 | 20.5 | 24 | 85.7 | 9.84 |
| | >90 | C | 30 | 48 | 1.4 | 6.7 | 1.93 | 0.07 | 0.03 | 4.61 | 0.64 | 19.5 | 27 | 86.0 | 10.1 |

*Note.* [1] Bulk density. [2] Organic carbon. [3] Cation exchange capacity. [4] Base saturation. [5] DCB-extractable

soils did not align with the characteristics of the typical soils found in ophiolite complexes, which were known for their low $SiO_2$ content (<45%) and relatively high $Fe_2O_3$ content. The low $SiO_2$ and high $Fe_2O_3$ content were inherited from the mafic and ultramafic parent materials (serpentinites), which are rich in Mg- and Fe- silicates (Hseu et al., 2007; Yang et al., 2022). However, the relatively high $SiO_2$ (>45%) and $Al_2O_3$ contents observed in the studied soils were indicative of their derivation from fine-grained sedimentary rocks, such as mudstone (Macquaker et al., 1997; Perri et al., 2021).

These rocks were primarily composed of clay minerals and silt-sized particles, which contained significant amounts of aluminosilicate minerals, including feldspars and micas. The presence of these minerals was confirmed through XRD analysis and cross-polarized light microscopy (Table 3; Figures 2 and 3).

Regarding the Ca/Mg ratio, the results revealed lower values in CP1, CP3, and CP4 pedons, all showing a ratio of less than or equal to 1.0 (Table 3). This outcome was likely influenced by the formation of carbonates, such as calcite, which developed after the parent materials in the ophiolite complex were formed (Dandar et al., 2023). Consequently, Ca tended to be depleted in the soils during weathering under a tropical humid climate (Nesbitt & Young, 1982; Harnois, 1988; Jiménez-Ballesta et al., 2022). In contrast, the subsurface horizons of the CP2 pedon exhibited a higher concentration of Ca compared to the total Mg concentration, which resulted in a Ca/Mg ratio exceeding 1.0. This elevated ratio in CP2, in comparison to the other pedons, was significantly influenced by the presence of feldspar and carbonate minerals (Nesbitt & Young, 1982). This was further supported by mineral micromorphology observed through polarized light microscopy, which indicated these minerals' contributions to the increased Ca levels in the CP2 pedon (Figures 2, 3a, and 3d). The intricate and diverse composition of the ophiolite complex created a unique mineralogical structure, which significantly contributed to the specific characteristics and behavior of this element. This relationship between the complexity of the mineral composition and the properties of the elements underscores the importance of the geological context in determining the distribution, concentration, and chemical behavior of the element within the ophiolite complex.

Ophiolitic soils are commonly enriched with trace metals, such as Cr, Ni, and Co, due to the presence of ultramafic rocks in the ophiolite complex (Kierczak et al., 2007; Oze et al., 2004; Kierczak et al., 2016; Hseu et al., 2018). Nevertheless, the formation of ophiolite complexes typically involved the accretion of sedimentary cover and other crustal layers, which led to lower concentrations of Cr, Ni, and Co in soils derived from these sedimentary parent materials (Kierczak et al., 2016; Hseu et al., 2018). In the studied ophiolitic soils, the concentrations of trace metals exhibited variations that ranged from 71.2 to 105.0 mg kg^{-1} for Cr, 23.6 to 43.2 mg kg^{-1} for Ni, and 20.3 to 27.9 mg kg^{-1} for Co (Table 3). Interestingly, the levels of Cr, Ni, and Co were slightly elevated in the CP3 pedon compared

Table 3
*Total contents of major and trace elements of the studied pedons*

| Pedon | Depth | Horizon | SiO₂ | Al₂O₃ | Fe₂O₃ | K₂O | Na₂O | CaO | MgO | MnO | Co | Cr | Ni | Ca/Mg |
|---|---|---|---|---|---|---|---|---|---|---|---|---|---|---|
| | cm | | | | | % | | | | | | mg kg⁻¹ | | |
| CP1 | 0–25 | A | 57.9 | 15.5 | 5.54 | 2.63 | 1.34 | 0.68 | 1.7 | 0.07 | 23.0 | 84.2 | 30.8 | 0.40 |
| | 25–45 | Bw1 | 60.5 | 16.2 | 5.84 | 2.65 | 1.35 | 0.58 | 1.84 | 0.06 | 24.3 | 95.1 | 35.3 | 0.31 |
| | 45–60 | Bw2 | 61.3 | 16.0 | 5.72 | 2.66 | 1.36 | 0.58 | 1.88 | 0.06 | 23.6 | 90.2 | 32.4 | 0.31 |
| | 60–85 | BC | 65.8 | 13.5 | 4.52 | 2.36 | 1.78 | 1.24 | 1.76 | 0.05 | 25.5 | 92.3 | 35.9 | 0.70 |
| | 85–105 | CB | 61.1 | 16.0 | 5.98 | 2.76 | 1.27 | 0.70 | 2.05 | 0.08 | 21.2 | 75.5 | 26.8 | 0.34 |
| | >105 | C | 62.4 | 14.9 | 5.30 | 2.60 | 1.56 | 1.36 | 2.11 | 0.07 | 23.9 | 85.0 | 30.8 | 0.65 |
| CP2 | 0–20 | A | 56.5 | 16.3 | 6.06 | 2.77 | 1.06 | 0.71 | 1.98 | 0.09 | 25.7 | 94.2 | 38.1 | 0.36 |
| | 20–45 | Bw1 | 56.1 | 16.7 | 6.45 | 2.89 | 1.01 | 1.89 | 2.24 | 0.10 | 26.7 | 100 | 37.5 | 0.84 |
| | 45–75 | Bw2 | 57.2 | 16.3 | 6.28 | 2.76 | 1.06 | 1.98 | 2.26 | 0.09 | 25.8 | 95.6 | 33.6 | 0.88 |
| | 75–100 | Bw3 | 57.0 | 16.5 | 6.33 | 2.78 | 1.14 | 1.97 | 2.28 | 0.09 | 26.5 | 97.2 | 36.4 | 0.87 |
| | 100–125 | BC | 59.2 | 15.5 | 5.88 | 2.6 | 1.19 | 2.25 | 2.25 | 0.09 | 25.3 | 91.9 | 32.2 | 1.00 |
| | >125 | C | 58.7 | 15.2 | 5.90 | 2.56 | 1.17 | 2.60 | 2.31 | 0.09 | 23.7 | 86.5 | 30.3 | 1.13 |
| CP3 | 0–15 | A | 59.3 | 15.6 | 5.82 | 2.52 | 1.17 | 0.77 | 1.73 | 0.09 | 25.9 | 96.8 | 36.5 | 0.45 |
| | 15–35 | Bw1 | 60.1 | 16.1 | 6.05 | 2.51 | 1.17 | 0.56 | 1.73 | 0.09 | 25.2 | 93.7 | 35.7 | 0.32 |
| | 35–55 | Bw2 | 58.8 | 16.1 | 6.09 | 2.53 | 1.14 | 0.58 | 1.77 | 0.09 | 25.2 | 95.5 | 35.8 | 0.33 |
| | 55–80 | BC | 53.2 | 16.2 | 6.22 | 2.55 | 0.96 | 0.67 | 1.90 | 0.09 | 27.9 | 105 | 43.2 | 0.36 |
| | 80–110 | CB | 57.9 | 16.6 | 6.21 | 2.65 | 1.10 | 0.74 | 1.90 | 0.08 | 26.4 | 103 | 40.6 | 0.39 |
| | >110 | C | 56.1 | 16.8 | 6.59 | 2.72 | 1.08 | 1.61 | 2.10 | 0.10 | 26.6 | 103 | 41.3 | 0.77 |
| CP4 | 0–15 | A | 60.8 | 14.2 | 5.16 | 2.39 | 1.41 | 0.73 | 1.51 | 0.08 | 23.8 | 84.1 | 31.3 | 0.48 |
| | 15–40 | Bw1 | 62.8 | 15.1 | 5.43 | 2.49 | 1.40 | 0.56 | 1.61 | 0.07 | 22.6 | 79.5 | 28.9 | 0.35 |
| | 40–60 | Bw2 | 62.8 | 15.1 | 5.41 | 2.48 | 1.40 | 0.59 | 1.59 | 0.08 | 20.2 | 71.2 | 26.6 | 0.37 |
| | 60–75 | BC | 63.9 | 14.9 | 5.28 | 2.44 | 1.45 | 0.61 | 1.55 | 0.08 | 23.7 | 85.2 | 30.8 | 0.39 |
| | 75–90 | CB | 64.0 | 14.7 | 5.15 | 2.41 | 1.46 | 0.59 | 1.52 | 0.07 | 23.7 | 83.2 | 30.6 | 0.39 |
| | >90 | C | 64.3 | 14.9 | 5.22 | 2.43 | 1.49 | 0.57 | 1.55 | 0.07 | 21.5 | 75.1 | 27.7 | 0.37 |

to the CP1, CP2, and CP4 pedons, which were situated in the lower backslope positions, respectively. Backslope areas were often considered zones of accumulation where eroded materials from upper slopes were deposited, leading to higher trace metal concentrations (Zhang et al., 2020). This observation was further supported by the fact that these higher concentrations of Cr, Ni, and Co in CP3 pedon corresponded with the elevated levels of DCB extractable Al and Fe in the same pedons, indicating the significant role of Fe- and Al-oxides in influencing the distribution of trace metals in the environment (Rinklebe & Shaheen, 2017; Merrot et al., 2021) (Tables 2 and 3).

The concentrations of Cr, Ni, and Co in the studied pedons (CP1 to CP4) were notably higher than the world soil averages of 59.5 mg kg$^{-1}$ for Cr, 29.0 mg kg$^{-1}$ for Ni, and 11.3 mg kg$^{-1}$ for Co (Kabata-Pendias, 2011), suggesting that these heavy metals accumulated during soil formation. However, when considering the implications for agricultural practices, the Cr, Ni, and Co levels in these soils were below the contamination control thresholds set for Taiwan, which were 175 mg kg$^{-1}$ for Cr and 130 mg kg$^{-1}$ for Ni, with no specific permissible limit for Co. The presence of minerals such as chlorite, serpentine, and chrysotile in the studied pedons (Figures 2, 3a, 3d, and 3e) further supported the idea that these elements were primarily of geogenic origin (Kierczak et al., 2007; Caillaud et al., 2009).

The trace metal levels found in this study were significantly lower than those reported in previous research, which was also conducted on ophiolite complexes in eastern Taiwan. For instance, Hseu et al. (2007) reported Cr concentrations (400 to 3,100 mg kg$^{-1}$) that were as far as thirty times higher, and Ni concentrations (400 to 5,800 mg kg$^{-1}$) were up to over a hundred times greater than those observed in this study. Similarly, Yang et al. (2022) reported that the Cr and Ni total concentrations ranged from 1,880 to 3,854 mg kg$^{-1}$ and 2,355 to 4,994 mg kg$^{-1}$, respectively. This discrepancy underscores the variability in trace metal concentrations across different ophiolite complexes, likely due to the fact that the studied soils are being partially derived from other parent materials as indicated by the higher Si content, the elevated concentration Al over Fe, and the limited presence of primary minerals responsible for the high concentration of trace metals. There was no data for the concentration of Co in the mentioned studies in Taiwan, but Kierczak (2016) reported that the total concentration of the element in Poland ranged from 83 to 168 mg kg$^{-1}$, much higher than the studied ophiolitic soils.

## Relationships Between Soil Properties, Major Elements, and Trace Metals

The geochemical characteristics of trace metals in ophiolitic soils were analyzed using Pearson's correlation to investigate their relationships with basic soil properties, major elements, and trace metals to better comprehend their solubility and mobility (Table 4). No significant correlation was observed between soil pH and the concentrations of Cr, Ni, and Co in the ophiolitic soils (Table 4). Even though higher concentrations of trace metals

were observed in CP2 and CP3 pedons, the soil pH values remained relatively consistent across different horizons and pedons (Tables 2 and 3). The studied ophiolitic soils were classified as Inceptisols, which exhibit comparable acidic to moderate pH values, causing the lack of relationships between soil pH and the trace metals. As these soils continue to develop, the influence of pedogenic processes on trace metal distribution is expected to become more pronounced.

Generally, besides pH, OC and Fe/Al-oxides were also the critical factors that influence the oxidation states and solubility of these trace metals, affecting their distribution and mobility (Hseu et al., 2018; Wang et al., 2020; Xu et al., 2020). OC generally provides retention sites and controls the movement of absorbed trace metals in soils (Wang et al., 2020). However, in this study, no significant correlations were found between OC and the concentrations of Cr, Ni, and Co, suggesting that the distribution of these trace metals may be influenced by factors other than OC (Table 4). The highest concentrations of trace metals were observed in the BC horizon of pedon CP3, with values of 105 mg kg$^{-1}$ for Cr, 43.2 mg kg$^{-1}$ for Ni, and 27.9 mg kg$^{-1}$ for Co. In contrast, the lowest values were recorded in the Bw2 horizon (71.2 mg kg$^{-1}$ for Cr, 20.2 mg kg$^{-1}$ for Co) and the C horizon (27.7 mg kg$^{-1}$ for Ni) of the CP4 pedon. Interestingly, both the highest (5.43% OC) and lowest (1.31% OC) levels of OC were found in the CP4 pedon, highlighting the variability in OC distribution across different soil horizons. The observed differences in the distributions of Cr, Ni, Co, and OC were likely associated with the strong affinity of these trace metals for Fe and Al oxides, which incorporate them into the mineral matrix rather than associating them with OM (Hseu et al., 2018; Wang et al., 2020; Xu et al., 2020).

The strong positive correlation between Fe$_t$ and Al$_t$ with Cr$_t$ ($p < 0.01$) and the positive correlations of these total elements with Ni$_t$ and Co$_t$ ($p < 0.05$) indicated a significant influence of the parent material and the geochemical affinity between these trace metals and the Fe and Al oxides present in the soils. The considerably elevated concentrations of total Al and Fe and the DCB-extractable Fe in the B horizons (79.7 to 88.3 g kg$^{-1}$ Fe$_t$; 37.8 to 45.1 g kg$^{-1}$ Al$_t$; 78.4 to 94.7 g kg$^{-1}$ Fe$_d$; Tables 2 and 3) strengthen the relationships of these elements with Cr, Ni, and Co. The high surface areas and reactive sites of Fe and Al oxides facilitate the adsorption of trace metals, leading to their co-precipitation with Cr, Ni, and Co (Bolaños-Benitez et al., 2021; Cornell & Schwertmann, 2003; Merrot et al., 2021). Pedogenic metal oxides, particularly Fe and Al oxides, were considered important sinks for trace metals in soils (Hseu, 2018). Moreover, the slightly to moderately acidic conditions of the studied soils (pH 6.06 to 6.88) likely played a role in the formation of these oxides (Schwertmann et al., 2000), as their pH-dependent solubility affects the availability of trace metals in the soil solution, leading to their accumulation in association with Fe and Al oxides (Table 2) (Bolaños-Benitez et al., 2021; Merrot et al., 2021). Among the trace metals studied, only Ni showed a positive correlation with Fe$_d$ ($p < 0.05$) in the

Table 4

*Pearson's correlation matrix among selected soil properties, selected total major elements, and total trace metals in the studied soil samples (n=24)*

|  | pH | OC | $Fe_d$ | $Al_d$ | $Si_t$ | $Al_t$ | $Fe_t$ | $Cr_t$ | $Ni_t$ | $Co_t$ | Ca/Mg |
|---|---|---|---|---|---|---|---|---|---|---|---|
| pH |  |  |  |  |  |  |  |  |  |  |  |
| OC | -0.43[*] |  |  |  |  |  |  |  |  |  |  |
| $Fe_d$ | 0.21 | -0.04 |  |  |  |  |  |  |  |  |  |
| $Al_d$ | 0.21 | 0.01 | 0.52[*] |  |  |  |  |  |  |  |  |
| $Si_t$ | 0.02 | -0.48[*] | -0.32 | 0.10 |  |  |  |  |  |  |  |
| $Al_t$ | 0.25 | 0.11 | 0.39 | 0.01 | -0.77[***] |  |  |  |  |  |  |
| $Fe_t$ | 0.19 | 0.19 | 0.42[*] | -0.15 | -0.86[***] | 0.95[***] |  |  |  |  |  |
| $Cr_t$ | 0.23 | 0.22 | 0.40 | 0.06 | -0.69[***] | 0.56[**] | 0.60[**] |  |  |  |  |
| $Ni_t$ | 0.26 | 0.25 | 0.43[*] | 0.23 | -0.66[***] | 0.50[*] | 0.51[*] | 0.95[***] |  |  |  |
| $Co_t$ | 0.21 | 0.23 | 0.34 | -0.03 | -0.65[***] | 0.43[*] | 0.50[*] | 0.97[***] | 0.93[***] |  |  |
| Ca/Mg | -0.26 | -0.01 | -0.19 | -0.84[***] | -0.22 | -0.02 | 0.18 | 0.21 | 0.01 | 0.29 |  |

*Note*. $Fe_d$: Fe DCB-extractable; $Al_d$: Al DCB-extractable. $Si_t$: total $SiO_2$; $Al_t$: total $Al_2O_3$; $Fe_t$: total $Fe_2O_3$; $Cr_t$: total Cr; $Ni_t$: total Ni; $Co_t$: total Co. *, **, and *** Significant at $p < 0.05$, 0.01, and 0.001

DCB extractable fraction, further emphasizing the role of free Fe oxides in influencing Ni distribution.

The Ca/Mg ratio is another important indicator that provides insights into the geological history and processes influencing the formation and evolution of ophiolites. This ratio is particularly useful in understanding the enrichment and depletion of basic cations through hydrothermal alteration processes (Miyashiro et al., 1969; Coleman & Keith, 1971; Hseu et al., 2018). The interactions between oceanic fluids and primary minerals during these processes can lead to the enrichment and incorporation of trace metals into the mineral structure (Naldrett & Lehmann, 1988; Grieco et al., 2004). As ophiolitic parent materials weather, they release major elements and trace metals, which become incorporated into the developing soil (Hseu et al., 2018). As soil development progresses, Ca is recycled by plants, while Mg is lost due to its solubility in the soil environment, which also affects the concentrations of Cr and Ni (Hseu, 2018). However, in this study, no significant correlations were observed between the Ca/Mg ratio and the concentrations of Cr, Ni, and Co in the ophiolitic soils (Figure 5), suggesting that the behavior of Ca and Mg during pedogenesis may have an indirect impact on trace metal concentrations rather than a direct one.

The study also revealed strong positive and significant correlations among $Cr_t$, $Ni_t$, and $Co_t$ ($p < 0.001$), indicating that these trace metals were concurrently released during the weathering of the ophiolitic parent material and were not significantly influenced by non-geogenic sources. In typical ophiolitic environments, where ultramafic rocks are the dominant source of soil development, Ni is often found in the structures of minerals located in octahedral layers, such as lizardite, antigorite, chrysotile, and other phyllosilicate

minerals, including those in the chlorite group. These minerals can be easily released during soil formation (Hseu et al., 2007; Kierczak et al., 2016). Cr and Co, on the other hand, are primarily sourced from chromite, a key mineral in ultramafic rocks, and are often enriched by magnetite (Oze et al., 2004; Kierczak et al., 2016; Hseu, 2018; Hseu et al., 2018; Yang et al., 2022). The weathering of the abovementioned minerals has a significant impact on the proportions of Cr, Ni, and Co in sediment-derived ophiolitic soils, such as those derived from mudstone. For instance, Garver et al. (1996) reported that elevated concentrations of trace metals in soils suggest the presence of ultramafic rocks in the sediment source region. While the origin of trace metals is often determined using background concentrations, world average elemental equivalence, and Earth's crust composition, the significant correlations between these trace metals and their abundance in ophiolitic soils also provide valuable provenance information, as they reflect the lithological characteristics of their parent materials (Tables 3 and 4) (Gonnelli & Renella, 2012; Kabata-Pendias, 2011).

## Mobility of Soil Components

The enrichments and depletion factors of clay, along with elements like Si, Al, Fe, Ca, Mg, and trace metals, were carefully analyzed to understand the long-term weathering rates of soils. The mass transfer coefficient ($\tau$) of clay increased significantly at the surface of the studied pedons, especially for the CP1 (summit; $Clay_\tau = 0.24$) and CP2 (upper backslope; $Clay_\tau = 0.23$) pedons, where the stability of the landscape allowed for intense chemical weathering over time, leading to the gradual build-up of clay, suggesting that the landscape has remained stable enough to favor clay accumulation. In contrast, in CP3 to CP4 pedons (lower backslope to the footslope; CP3, $Clay_\tau = 0.09$; CP4, $Clay_\tau = 0.10$), in consideration of the increasing slope, the enrichment of clay might be mainly due to erosion and deposition processes. These processes have moved clay particles from higher areas to lower ones, resulting in sediment accumulation and a corresponding increase in clay content in these pedons. In terms of the subsurface horizons, both pedons CP1 and CP2 generally had similar increases in clay content ($Clay_\tau = 0.00$ to $0.02$), suggesting the constant accumulation of clay particles. CP3 pedon ($Clay_\tau = -0.01$ to $0.02$), however, generally showed no significant gains or losses in the subsurface horizons, indicating a balance between erosion and deposition. On the other hand, CP4 pedon ($Clay_\tau = -0.19$ to $0.04$) experienced a noticeable loss of clay in the subsurface layers, which is likely due to water percolation that leaches clay particles away, leaving behind coarser materials (Table 2).

Similar patterns were observed for the major elements Si, Al, and Fe, which correlated with the clay content, indicating that the behavior of these major elements appears to be interrelated, likely due to the influence of soil formation processes, particularly the translocation of secondary clay minerals within the soil profiles (Tonkha et al., 2021). The accumulation of major elements in the surface horizon in CP1 to CP4 pedons ($Si_\tau = 0.10$ to

0.21; $Al_\tau =$ 0.09 to 0.21; $Fe_\tau =$ 0.09 to 0.20) is probably due to the higher concentration of fine particles, while the losses of these elements in the subsurface horizons, especially in CP4 pedon ($Si_\tau =$ -0.18 to 0.04; $Al_\tau =$ -0.19 to 0.04; $Fe_\tau =$ -0.19 to 0.04), may be attributed to coarser or less uniform textures (Macquaker et al., 1997; Tonkha et al., 2021). CP1 ($Ca_\tau =$ 0.00 to 0.15; $Mg_\tau =$ 0.00 to 0.18), CP2 ($Ca_\tau =$ 0.00 to 0.11; $Mg_\tau =$ 0.00 to 0.16), CP3 ($Ca_\tau =$ 0.00 to 0.05; $Mg_\tau =$ 0.00 to 0.08) pedons, and the surface soils of CP4 ($Ca_\tau =$ 0.14; $Mg_\tau =$ 0.10) exhibited no net gain and loss to positive mass fluxes for Ca and Mg (Figure 4). Typically, in ophiolitic soils, the behavior of these basic cations changes as soil development progresses. Mg is often leached out through the breakdown of Mg-silicate minerals and high-activity clay minerals, while Ca tends to be recycled by plants (Hseu, 2018; Yang et al., 2022). However, in this study, both Ca and Mg showed comparable mass fluxes, which is consistent with the intermediate stage of soil development observed in the studied ophiolitic soils (Table 1).

The selected trace metals in the ophiolitic soils exhibited similar mass flux patterns, indicating consistent geochemical behavior and uniformity in the source material (Figure 5). Notable positive mass fluxes were observed in surface and upper subsurface soils from pedons CP1 ($Cr_\tau =$ 0.14 to 0.24; $Ni_\tau =$ 0.14 to 0.25; $Co_\tau =$ 0.13 to 0.24) and CP2 ($Cr_\tau =$ 0.04 to 0.20; $Ni_\tau =$ 0.04 to 0.23; $Co_\tau =$ 0.04 to 0.20), as well as in the surface soils of pedons CP3 ($Cr_\tau =$ 0.11; $Ni_\tau =$ 0.10; $Co_\tau =$ 0.11) and CP4 ($Cr_\tau =$ 0.14; $Ni_\tau =$ 0.14; $Co_\tau =$ 0.14), suggesting an enrichment of these metals in the upper soil layers. Conversely, the subsurface horizons of pedon CP4 displayed negative mass fluxes, indicating a loss of trace metals in the soils from low-elevation areas. The observed gains and losses of trace metals in the studied ophiolitic soils (CP1 to CP4 pedons) corresponded closely with the behavior of the major elements, such as Al, Fe, and clay. These elements are known to provide retention sites for trace metals, effectively controlling their mobility and availability within the soil matrix (Bolaños-Benitez et al., 2021; Cornell & Schwertmann, 2003; Merrot et al., 2021; Hseu et al., 2018; Wang et al., 2020).

Specifically, the positive correlations between trace metals and Fe and Al in the studied ophiolitic soils (Table 4), along with the substantially elevated concentrations of total and DCB extractable Al and Fe in B horizons (Tables 2 & 3) as mentioned above, reinforced the idea that these elements played a critical role in the accumulation of metals, particularly Cr, Ni, and Co. Although OC did not exhibit a direct positive correlation with the trace metals (Table 4), the high concentrations of OC in the surface soils still reflect the observed gains of trace metals in these horizons, which serves as binding agents that enhance trace metal retention (Wang et al., 2020; Table 2; Figure 5). Furthermore, the noticeable change in the mass flux of trace metals was observed only in pedon CP4, which exhibited a negative trend in the subsurface horizons, likely influenced by the higher proportion of coarse particles (25 to 40% sand; Table 2; Figure 5). Coarse-textured soils,

with their higher permeability, tend to promote the mobility and leaching of trace metals. Additionally, the elevated concentrations of trace metals in the surface soils of the studied pedons might be attributed to the higher OC content, which can bind trace metals and enhance their retention (Table 2).

The observed behavior of trace metals in these ophiolitic soils did not align with findings from previous studies, which suggested that trace metals tend to accumulate more at lower elevations due to longer water residence time (Chen & Torres, 2012; Liu et al., 2016). This discrepancy suggested that other soil components, such as texture and OM, may play a more significant role in determining trace metal distribution than elevation alone. Moreover, the behavior of clay content, major elements, and trace metals in the studied ophiolitic soils followed similar trends, reinforcing that the parent material and pedogenesis primarily influence these soil components. Furthermore, the consistency across these elements suggested that external factors, particularly anthropogenic inputs, did not significantly impact the observed patterns but rather reflected the intrinsic characteristics of the soil and its natural development over time.
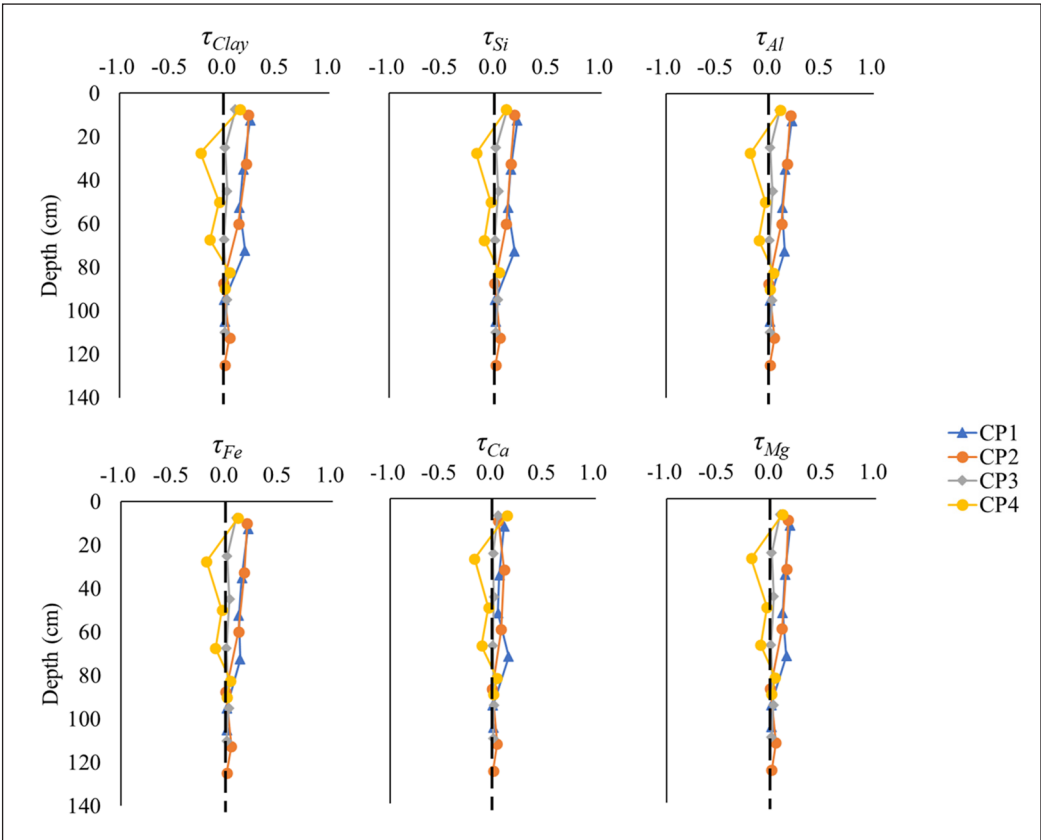


*Figure 4*. Mass transport coefficient ($\tau$) of clay, Si, Al, Fe, Ca, and Mg with depth

1010

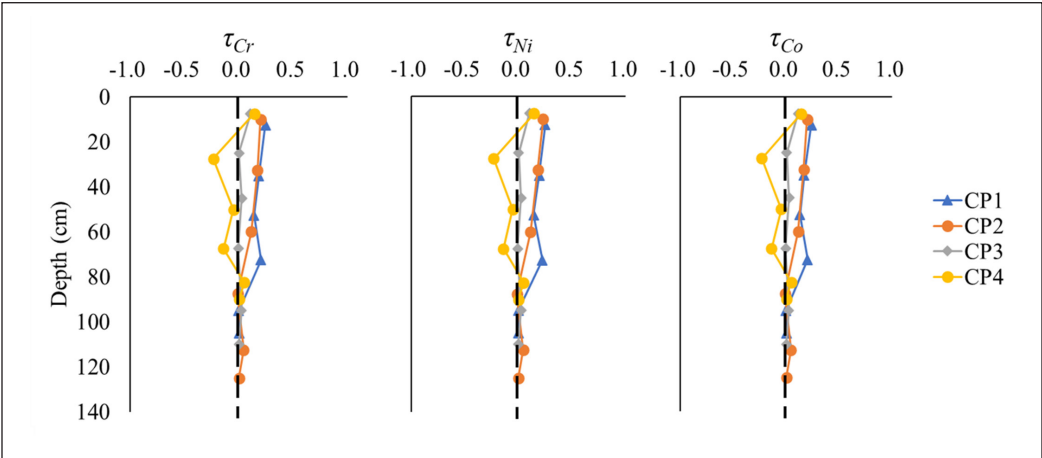Pertanika J. Trop. Agric. Sci. 48 (3): 991 - 1017 (2025)

*Figure 5.* Mass transport coefficient (τ) of Cr, Ni, and Co with depth

## CONCLUSION

The study provided a comprehensive understanding of their mineralogical and geochemical properties, highlighting the intricate relationships between soil formation processes and trace metal dynamics. The study identified key minerals such as chlorites, feldspars, and quartz, which reflect that the studied soils were not derived from typical ophiolite parent materials (serpentine) but rather mudstones. It also revealed that the concentrations of trace metals, including Cr, Ni, and Co, were influenced significantly by the presence of Fe and Al oxides. Moreover, the mobility and retention of trace metals in the studied pedons are closely linked to soil texture, suggesting that well-drained, coarse-textured soils may facilitate leaching. The accumulation of trace metals in CP1, CP2, and CP3 pedons (summit and upper backslope) rather than in CP4 (footslope) emphasized the need to consider local soil characteristics and environmental factors in understanding trace metal behavior. Additionally, the results emphasized the variability in trace metal concentrations across different pedons in the ophiolite complex, which was attributed to other parent materials and soil formation processes. Furthermore, the exploration of the relationships between trace metals and soil components highlighted the complex interactions that govern their mobility, emphasizing the need for a nuanced understanding of soil dynamics in these unique environments and providing valuable insights for future research and land management practices.

## ACKNOWLEDGMENTS

also like to acknowledge the support of the Department of Science and Technology—Science Education Institute through the DOST-SEI Foreign Graduate Scholarships in Specialized Priority Fields in Science and Technology.

## REFERENCES

Baralkiewicz, D., & Siepak, J. (1999). Chromium, nickel and cobalt in environmental samples and existing legal norms. *Polish Journal of Environmental Studies*, *8*(4), 201-208.

Bédard, É., Hébert, R., Guilmette, C., & Dostal, J. (2008). The supra-ophiolitic sedimentary cover of the Asbestos ophiolite, Québec, Canada: First geochemical evidence of transition from oceanic to continental sediment flux. *Lithos*, *105*(3–4), 239–252. https://doi.org/10.1016/j.lithos.2008.04.005

Blake, G. R., & Hartge, K. H. (1986). Bulk density. In A. K. Klute (Ed.), *Methods of soil analysis: Part 1, physical and mineralogical methods* (pp. 363–375). Academic Press. https://doi.org/10.2136/sssabookser5.1.2ed.c13

Bolaños-Benítez, V., Van Hullebusch, E., Birck, J., Garnier, J., Lens, P. N., Tharaud, M., Quantin, C., & Sivry, Y. (2021). Chromium mobility in ultramafic areas affected by mining activities in Barro Alto massif, Brazil: An isotopic study. *Chemical Geology*, *561*, 120000. https://doi.org/10.1016/j.chemgeo.2020.120000

Brimhall, G. H., & Dietrich, W. E. (1987). Constitutive mass balance relations between chemical composition, volume, density, porosity, and strain in metasomatic hydrochemical systems: Results on weathering and pedogenesis. *Geochimica Et Cosmochimica Acta*, *51*(3), 567–587. https://doi.org/10.1016/0016-7037(87)90070-6

Brimhall, G. H., Chadwick, O. A., Lewis, C. J., Compston, W., Williams, I. S., Danti, K. J., Dietrich, W. E., Power, M. E., Hendricks, D., & Bratt, J. (1992). Deformational mass transport and invasive processes in soil evolution. *Science*, *255*(5045), 695–702. https://doi.org/10.1126/science.255.5045.695

Caillaud, J., Proust, D., Philippe, S., Fontaine, C., & Fialin, M. (2009). Trace metals distribution from a serpentinite weathering at the scales of the weathering profile and its related weathering microsystems and clay minerals. *Geoderma*, *149*(3–4), 199–208. https://doi.org/10.1016/j.geoderma.2008.11.031

Chadwick, O. A., Brimhall, G. H., & Hendricks, D. M. (1990). From a black to a gray box — A mass balance interpretation of pedogenesis. *Geomorphology*, *3*(3–4), 369–390. https://doi.org/10.1016/0169-555x(90)90012-f

Chapman, S. L., & Horn, M. E. (1968). Parent material uniformity and origin of silty soils in northwest arkansas based on zirconium-titanium contents. *Soil Science Society of America Journal*, *32*(2), 265-271. https://doi.org/10.2136/sssaj1968.03615995003200020030x

Chen, S., & Torres, R. (2012). Effects of geomorphology on the distribution of metal abundance in salt marsh sediment. *Estuaries and Coasts*, *35*(4), 1018–1027. https://doi.org/10.1007/s12237-012-9494-y

Cheng, C., Jien, S., Tsai, H., Chang, Y., Chen, Y., & Hseu, Z. (2009). Geochemical element differentiation in serpentine soils from the Ophiolite Complexes, eastern Taiwan. *Soil Science*, *174*(5), 283–291. https://doi.org/10.1097/ss.0b013e3181a4bf68

Coleman, R. G., & Keith, T. E. (1971). A chemical study of serpentinization--Burro Mountain, California. *Journal of Petrology*, *12*(2), 311–328. https://doi.org/10.1093/petrology/12.2.311

Cornell, R. M., & Schwertmann, U. (2003). *The iron oxides: structure, properties, reactions, occurrences and uses* (2nd ed.). Wiley. http://doi.org/10.1002/3527602097

Da Silva, Y. J. A. B., Nascimento, C. W. A. D., Biondi, C. M., Van Straaten, P., Da Silva, Y. J. A. B., De Souza, V. S., De Araújo, J. D. C. T., Alcantara, V. C., Da Silva, F. L., & Da Silva, R. J. A. B. (2020). Concentrations of major and trace elements in soil profiles developed over granites across a climosequence in northeastern Brazil. *Catena*, *193*, 104641. https://doi.org/10.1016/j.catena.2020.104641

Dandar, O., Okamoto, A., Uno, M., & Tsuchiya, N. (2023). Mantle hydration initiated by Ca metasomatism in a subduction zone: An example from the Chandman meta-peridotite, western Mongolia. *Lithos*, *452–453*, 107212. https://doi.org/10.1016/j.lithos.2023.107212

Deer, W. A., Howie, R. A., & Zussman, J. (2013). *An introduction to the rock-forming minerals* (3rd ed.). Berforts Information Press. https://doi.org/10.1180/dhz

Dilek, Y., & Furnes, H. (2014). Ophiolites and their origins. *Elements*, *10*(2), 93–100. https://doi.org/10.2113/gselements.10.2.93

DiPietro, J. A. (2013). Keys to the interpretation of Geological history. In J. A. DiPietro (Ed.), *Landscape evolution in the United States: An introduction to the geography, geology, and natural history* (pp. 327–344). Elsevier. https://doi.org/10.1016/b978-0-12-397799-1.00020-8

Egli, M., Mirabella, A., & Sartori, G. (2008). The role of climate and vegetation in weathering and clay mineral formation in late Quaternary soils of the Swiss and Italian Alps. *Geomorphology*, *102*(3–4), 307–324. https://doi.org/10.1016/j.geomorph.2008.04.001

Garver, J. I., Royce, P. R., & Smick, T. A. (1996). Chromium and nickel in shale of the taconic foreland: A case study for the provenance of fine-grained sediments with an ultramafic source. *Journal of Sedimentary Research*, *66*(1), 100–106. https://doi.org/10.1306/d42682c5-2b26-11d7-8648000102c1865d

Gawlick, H., & Missoni, S. (2019). Middle-late Jurassic sedimentary mélange formation related to ophiolite obduction in the Alpine-Carpathian-Dinaridic Mountain Range. *Gondwana Research*, *74*, 144–172. https://doi.org/10.1016/j.gr.2019.03.003

Gee, G. W., & Bauder, J. W. (1986). Particle-size analysis. In A. K. Klute (Ed.), *Methods of soil analysis: Part 1, physical and mineralogical methods* (pp. 383–411). Academic Press. https://doi.org/10.2136/sssabookser5.1.2ed.c15

Gonnelli, C., & Renella, G. (2012). Chromium and nickel. In B. J. Alloway (Ed.), *Heavy metals in soils: Trace metals and metalloids in soils and their bioavailability* (pp. 313–333). Springer. https://doi.org/10.1007/978-94-007-4470-7_11

Grieco, G., Ferrario, A., & Mathez, E. A. (2004). The effect of metasomatism on the Cr-PGE mineralization in the Finero Complex, Ivrea Zone, Southern Alps. *Ore Geology Reviews*, *24*(3–4), 299–314. https://doi.org/10.1016/j.oregeorev.2003.05.004

Harnois, L. (1988). The CIW index: A new chemical index of weathering. *Sedimentary Geology*, *55*(3–4), 319–322. https://doi.org/10.1016/0037-0738(88)90137-6

Ho, C. (1988). *An introduction to the geology of Taiwan: Explanatory text of the geologic map of Taiwan*. Central Geological Survey, Ministry of Economic Affairs. http://ci.nii.ac.jp/ncid/BA17266618

Hseu, Z. Y. (2018). Element enrichment in serpentine soils. In Z. Y. Hseu (Ed.), *Biogeochemistry of serpentine soils* (pp. 61–90). Nova Science Publisher. https://doi.org/10.1201/9781315154664-8

Hseu, Z. Y., Tsai, H., Hsi, H. C., & Chen, Y. C. (2007). Weathering sequences of clay minerals in soils along a serpentinitic toposequence. *Clays and Clay Minerals*, *55*(4), 389–401. https://doi.org/10.1346/ccmn.2007.0550407

Hseu, Z., Zehetner, F., Fujii, K., Watanabe, T., & Nakao, A. (2018). Geochemical fractionation of chromium and nickel in serpentine soil profiles along a temperate to tropical climate gradient. *Geoderma*, *327*, 97–106. https://doi.org/10.1016/j.geoderma.2018.04.030

Hum, H. Z., Huang, W., & Hseu, Z. (2024). Pedogenic characterization of rare earth elements in humid subtropical soils on volcanic plateaus. *Catena*, *244*, 108256. https://doi.org/10.1016/j.catena.2024.108256

Ito, A., Otake, T., Maulana, A., Sanematsu, K., Sufriadin, N., & Sato, T. (2021). Geochemical constraints on the mobilization of Ni and critical metals in laterite deposits, Sulawesi, Indonesia: A mass-balance approach. *Resource Geology*, *71*(3), 255–282. https://doi.org/10.1111/rge.12266

Jiménez-Ballesta, R., Bravo, S., García-Pradas, J., Pérez-de-los-Reyes, C., Amorós, J. A., & García-Navarro, F. J. (2022). Characteristics of vineyard soils derived from Plio-Quaternary landforms (raña or rañizo) in southern Europe. *European Journal of Soil Science*, *73*(4), e13291. https://doi.org/10.1111/ejss.13291

Jiménez-Ballesta, R., Bravo, S., Pérez-De-Los-Reyes, C., Amorós, J. A., Villena, J., & García-Navarro, F. J. (2024). Pedological formations on old mountain geomorphological surfaces of central Spain. *Heliyon*, *10*(1), e23852. https://doi.org/10.1016/j.heliyon.2023.e23852

Kabata-Pendias, A. (2011). *Trace elements in soils and plants* (4th ed.). CRC Press. https://doi.org/10.1201/b10158

Kierczak, J., Neel, C., Bril, H., & Puziewicz, J. (2007). Effect of mineralogy and pedoclimatic variations on Ni and Cr distribution in serpentine soils under temperate climate. *Geoderma*, *142*(1–2), 165–177. https://doi.org/10.1016/j.geoderma.2007.08.009

Kierczak, J., Pędziwiatr, A., Waroszewski, J., & Modelska, M. (2016). Mobility of Ni, Cr and Co in serpentine soils derived on various ultrabasic bedrocks under temperate climate. *Geoderma*, *268*, 78–91. https://doi.org/10.1016/j.geoderma.2016.01.025

Külah, T., Kadir, S., Gürel, A., Eren, M., & Önalgil, N. (2014). Mineralogy, geochemistry, and genesis of mudstones in the Upper Miocene Mustafapaşa member of the Ürgüp Formation in the Cappadocia region, central Anatolia, Turkey. *Clays and Clay Minerals*, *62*(4), 267–285. https://doi.org/10.1346/ccmn.2014.0620403

Lazar, O. R., Bohacs, K. M., Macquaker, J. H. S., Schieber, J., & Demko, T. M. (2015). Capturing key attributes of fine-grained sedimentary rocks in outcrops, cores, and thin sections: Nomenclature and description guidelines. *Journal of Sedimentary Research*, *85*(3), 230–246. https://doi.org/10.2110/jsr.2015.11

Liu, H., Xiong, Z., Jiang, X., Liu, G., & Liu, W. (2016). Heavy metal concentrations in riparian soils along the Han River, China: The importance of soil properties, topography and upland land use. *Ecological Engineering*, *97*, 545–552. https://doi.org/10.1016/j.ecoleng.2016.10.060

Ma, Y., & Hooda P. S. (2010). Chromium, nickel and cobalt. In P. S. Hooda (Ed.), *Trace elements in soils* (1st ed., pp. 461-479). Blackwell Publishing Ltd. http://doi.org/10.1002/9781444319477.ch19

Macquaker, J. H. S., Curtis, C. D., & Coleman, M. L. (1997). The role of iron in mudstone diagenesis: Comparison of Kimmeridge Clay Formation Mudstones from Onshore and Offshore (UKCS) Localities. *Journal of Sedimentary Research*, *67*(5), 871–878. https://doi.org/10.1306/d426865d-2b26-11d7-8648000102c1865d

Mclean, E. O. (1982). Soil pH and lime requirement. In A. L. Page (Ed.), *Methods of soil analysis: Part 2, chemical and microbiological properties* (2nd ed., pp. 199–224). Academic Press. https://doi.org/10.2134/agronmonogr9.2.2ed.c12

Mehra, O., & Jackson, M. (2013). Iron oxide removal from soils and clays by a dithionite–citrate system buffered with sodium bicarbonate. In E. Ingerson (Ed.), *Clays and clay minerals: Proceedings of the seventh national conference on clays and clay minerals* (pp. 317–327). Pergamon Press. https://doi.org/10.1016/b978-0-08-009235-5.50026-7

Merrot, P., Juillot, F., Pape, P. L., Lefebvre, P., Brest, J., Kieffer, I., Menguy, N., Viollier, E., Fernandez, J., Moreton, B., Radakovitch, O., & Morin, G. (2021). Comparative Cr and Mn speciation across a shore-to-reef gradient in lagoon sediments downstream of Cr-rich Ferralsols upon ultramafic rocks in New Caledonia. *Journal of Geochemical Exploration*, *229*, 106845. https://doi.org/10.1016/j.gexplo.2021.106845

Miyashiro, A., Shido, F., & Ewing, M. (1969). Composition and origin of serpentinites from the Mid-Atlantic Ridge near 24° and 30° North Latitude. *Contributions to Mineralogy and Petrology*, *23*(2), 117–127. https://doi.org/10.1007/bf00375173

Morrison, J. M., Goldhaber, M. B., Mills, C. T., Breit, G. N., Hooper, R. L., Holloway, J. M., Diehl, S. F., & Ranville, J. F. (2015). Weathering and transport of chromium and nickel from serpentinite in the Coast Range ophiolite to the Sacramento Valley, California, USA. *Applied Geochemistry*, *61*, 72–86. https://doi.org/10.1016/j.apgeochem.2015.05.018

Naldrett, A. J., & Lehmann, J. (1988). Spinel non-stoichiometry as the explanation for NI-, CU- and PGE-enriched sulphides in chromitites. In H. M. Prichard, P. J. Potts, J. F. W. Bowles & S. J. Cribb (Eds.), *Geo-Platinum 87* (pp. 93–109). Elsevier Science Publishers. https://doi.org/10.1007/978-94-009-1353-0_10

Nelson, D. W., & Sommers, L. E. (1982). Total carbon, organic carbon, and organic matter. In A. L. Page (Ed.), *Methods of soil analysis: Part 2, chemical and microbiological properties* (pp. 961-1010). Academic Press. https://doi.org/10.2134/agronmonogr9.2.2ed.c29

Nesbitt, H. W., & Young, G. M. (1982). Early Proterozoic climates and plate motions inferred from major element chemistry of lutites. *Nature*, *299*(5885), 715–717. https://doi.org/10.1038/299715a0

Oze, C., Fendorf, S., Bird, D. K., & Coleman, R. G. (2004). Chromium geochemistry in serpentinized ultramafic rocks and serpentine soils from the Franciscan complex of California. *American Journal of Science, 304*, 67–101. https://doi.org/10.2475/ajs.304.1.67

Perri, F., Milli, S., Campilongo, G., Tentori, D., & Critelli, S. (2021). The mudstone composition as reflected in the sedimentary evolution of a turbidite basin: The example of the Agnone Flysch (Molise, Italy). *Marine and Petroleum Geology*, *132*, 105241. https://doi.org/10.1016/j.marpetgeo.2021.105241

Rhoades, J. (1982). Cation exchange capacity. In A. L. Page (Ed.), *Methods of soil analysis: Part 2, chemical and microbiological properties* (2nd ed., pp. 149–157). Academic Press. https://doi.org/10.2134/agronmonogr9.2.2ed.c8

Rinklebe, J., & Shaheen, S. M. (2017). Redox chemistry of nickel in soils and sediments: A review. *Chemosphere*, *179*, 265–278. https://doi.org/10.1016/j.chemosphere.2017.02.153

Robertson, A. H., Palak, O., Tasli, K., & Dumitrica, P. (2020). Processes of clastic sedimentation associated with Late Cretaceous ophiolite emplacement in the SW segment of the Antalya Complex (S Turkey). *Sedimentary Geology*, *408*, 105718. https://doi.org/10.1016/j.sedgeo.2020.105718

Schwertmann, U., Friedl, J., Stanjek, H., & Schulze, D. G. (2000). The effect of Al on Fe Oxides. XIX. Formation of Al-Substituted Hematite from Ferrihydrite at 25°C and pH 4 To 7. *Clays and Clay Minerals*, *48*(2), 159–172. https://doi.org/10.1346/ccmn.2000.0480202

Soil Science Division Staff. (2017). Examination and description of soils profiles. In *Soil Survey Manual* (pp. 83-234). USDA-Soil Conservation Service.

Soil Survey Staff. (2022). Inceptisols. In *Keys to Soil Taxonomy* (pp. 207-246). USDA Natural Resources Conservation Service.

Tazikeh, H., Khormali, F., Amini, A., & Motlagh, M. B. (2018). Geochemistry of soils derived from selected sedimentary parent rocks in Kopet Dagh, North East Iran. *Journal of Geochemical Exploration*, *194*, 52–70. https://doi.org/10.1016/j.gexplo.2018.07.008

Tonkha, O., Butenko, A., Bykova, O., Kravchenko, Y., Pikovska, O., Kovalenko, V., Evpak, I., Masyk, I., & Zakharchenko, E. (2021). Spatial heterogeneity of soil silicon in Ukrainian phaozems and chernozems. *Journal of Ecological Engineering*, *22*(2), 111–119. https://doi.org/10.12911/22998993/130884

U. S. Environmental Protection Agency. (2021). *Method 3052 – Microwave assisted acid digestion of siliceous and organically based matrices.* https://www.epa.gov/sites/default/files/2015-12/documents/3052.pdf

Ullah, R., & Muhammad, S. (2020). Heavy metals contamination in soils and plants along with the mafic–ultramafic complex (Ophiolites), Baluchistan, Pakistan: Evaluation for the risk and phytoremediation potential. *Environmental Technology and Innovation*, *19*, 100931. https://doi.org/10.1016/j.eti.2020.100931

Verrecchia, E. P., & Trombino, L. (2021). *A visual atlas for soil micromorphologists*. Springer. https://doi.org/10.1007/978-3-030-67806-7

Wang, Y., Tsou, M., Liao, H., Hseu, Z., Dang, W., Hsi, H., & Chien, L. (2020). Influence of soil properties on the bioaccessibility of Cr and Ni in geologic serpentine and anthropogenically contaminated non-serpentine soils in Taiwan. *The Science of the Total Environment*, *714*, 136761. https://doi.org/10.1016/j.scitotenv.2020.136761

Wu, C., & Hseu, Z. (2023). Pedochemical behaviors of rare earth elements in soil profiles along a lithosequence in eastern Taiwan. *Catena*, *225*, 107047. https://doi.org/10.1016/j.catena.2023.107047

Wu, W., Guan, Y., Nel, W., & Xu, C. (2024). Heavy metal migration and Lithium isotope fractionation under extreme weathering of basalt on tropical Hainan Island, China. *Applied Geochemistry*, *175*, 106163. https://doi.org/10.1016/j.apgeochem.2024.106163

Xu, T., Nan, F., Jiang, X., Tang, Y., Zeng, Y., Zhang, W., & Shi, B. (2020). Effect of soil pH on the transport, fractionation, and oxidation of chromium (III). *Ecotoxicology and Environmental Safety*, *195*, 110459. https://doi.org/10.1016/j.ecoenv.2020.110459

Yang, C., Nguyen, D., Ngo, H., Navarrete, I., Nakao, A., Huang, S., & Hseu, Z. (2022). Increases in Ca/Mg ratios caused the increases in the mobile fractions of Cr and Ni in serpentinite-derived soils in humid Asia. *Catena*, *216*, 106418. https://doi.org/10.1016/j.catena.2022.106418

Zhang, Y., Zhang, X., Bi, Z., Yu, Y., Shi, P., Ren, L., & Shan, Z. (2020). The impact of land use changes and erosion process on heavy metal distribution in the hilly area of the Loess Plateau, China. *The Science of the Total Environment*, *718*, 137305. https://doi.org/10.1016/j.scitotenv.2020.137305